MODEL DESCRIPTION

We use the mixed transport-limited and detachment-limited option (Whipple and Tucker, 2002) in the CHILD landscape evolution model (e.g., Tucker et al., [2001a, 2001b]) to calculate changes in the modeled topography. Changes in topography due to fluvial processes are limited by the slower, rate-limiting process:

$$\frac{dz(x,y)}{dt}_{(fluvial)} = max\left\{\frac{dz(x,y)}{dt}_{(d-lim)}, \frac{dz(x,y)}{dt}_{(t-lim)}\right\}. \text{ (equation 1)}$$

The first term in the brackets in Equation 1 is the detachment-limited incision rate, which is calculated as a power-law function of fluvial discharge, $Q(x,y)$, and channel slope, $S(x,y)$ (only applies where channel slope is positive), (e.g., Howard, 1994; Whipple and Tucker, 1999):

$$\frac{dz(x,y)}{dt}_{(d-lim)} = -KQ(x,y)^m S(x,y)^n, \text{ (equation 2)}$$

where m and n are dimensionless parameters and are fixed with the common values of 0.5 and 1.0, respectively, in all model experiments (e.g., Tucker and Whipple, 2002). The parameter K is a measure of rock erodibility. (Here K has units of meters^{1-3m}years^{m-1}.) The second term in brackets in Equation 1 is the transport-limited incision rate, which is calculated as the divergence of the sediment flux:

$$\frac{dz(x,y)}{dt}_{(t-lim)} = -\frac{dQ_t(x,y)}{dA(x,y)}, \text{ (equation 3)}$$

where Q_t is the volumetric sediment transport rate; A is the drainage area; and dA is the change in drainage area across a cell, or the cell area. Note that transport-limited processes can result in sediment deposition (Equation 3 can result in a positive value), which leads the calculation in Equation 1 to be positive and, as a result, the local elevation increases (the uplift rate is always either positive or zero in the experiments). The sediment transport rate is calculated as a power-law function of fluvial discharge and channel slope:

$$Q_t = K_t Q(x,y)^{m_t} S(x,y)^{n_t}, \text{ (equation 4)}$$

where m_t and n_t are dimensionless parameters and are fixed with the common values of 1.5 and 1.0, respectively, in all model experiments (Whipple and Tucker, 2002). The parameter K_t is a measure of transport efficiency, here with units of meters^{3-3mt}years^{mt-1}. The values of K and K_t are kept equal in all our simulations in order to mimic the expectations that steady-state channels are close to a transport-limited condition and largely covered by a thin layer of alluvium, and that detachment-limited conditions and the formation of discrete knickpoints or convexities will form in response to an increase in rock uplift rate, but that channels may be come transport limited if rock uplift rates decrease (e.g., Whipple and Tucker, 2002; Baldwin et al., 2003). This is the simplest model that could potentially capture the major controls on landscape evolution in the Bolivian Andes.

We explore the possibility that the difference between the high k_{sn} transverse channels and the frontal channels is due to lithology, and we model the potential difference of rock type by varying K and K_t in the numerical simulations. Values of K and K_t are set so that the slope values in the modeled channels are close to those in the Bolivian channels. In the Bolivian channels that drain the harder rocks, K and K_t are estimated to be 5e-7 (units differ for K and K_t, Equations 2 and 4). Based on the ratio between k_{sn} in the two frontal channels south of the BE (Fig. 7C from main text), only one of which drains a significant area of granitic rocks (Fig. 2B from main text), we increase the K-values by a factor of 1.8 (to 9e-7) in two of the simulations to explore whether this leads to a similar morphology as observed

in the frontal channels on the BE. This change in *K*-values is consistent with greater compressive strength of the granitic and high grade metamorphic rocks in comparison to the lower grade metasedimentary rocks (Safran, 1998; Aalto et al., 2006).

The upper convexities in the transverse channels could be enhanced by a lack of sediment supplied from the upstream reaches of the channel that are incising at lower rates (due to lower precipitation rates, or because this portion of the landscape has not yet responded to the increase in rock uplift rates) (Chatanantavet and Parker, 2006; Gasparini et al., 2007). The CHILD model contains an algorithm to model enhanced and suppressed bedrock incision rates from sediment tools and cover effects (Gasparini et al., 2007). However, we do not present results using this more complex model because it is not able to simulate convexities at large drainage areas, such as the convexities observed in the transverse channels (the model would be unstable). The lack of sediment tools may be responsible for convexities formed at hanging tributaries (Crosby et al., 2007), as is discussed for the region north- and southeast of the escarpment by Whipple and Gasparini (2014) and could serve to enhance channel steepness values immediately below transient convexities as is discussed qualitatively in the section .1 "Role of Tectonics, Rainfall, and Lithology on the Morphology of the Beni Escarpment" of the main text.

Discharge is modeled as the sum of all surface water from upstream contributing points:

$$Q(x,y) = \sum_i P(x_i,y_i)\, a(x_i,y_i), \text{ (equation 5)}$$

where $P(x_i,y_i)$ and $a(x_i,y_i)$ are the rainfall rate and local area of the cell surrounding the point at (x_i,y_i). Here the summation is over all points *i* upstream of and including the point (x,y). Equation 5 expresses how discharge is calculated within the model, but it reduces to $Q(x,y) = \bar{P}(x,y)A(x,y)$, where $A(x,y)$ is the upstream contributing drainage area at a point (x,y) and $\bar{P}(x,y)$ is the upstream spatially average rainfall rate.

We use two different rainfall scenarios in our numerical experiments. In the first scenario, the rainfall rate is uniform at 1,000 mm/yr. The second scenario, referred to as the non-uniform rainfall pattern, is based on the rainfall patterns observed across the BE (Fig. 2 from main text). We consider changes in rainfall rate only in the direction perpendicular to the mountain front, hence the rainfall rate varies only in the *y* direction. The rainfall pattern is divided into three distinct regions (Fig. 11D from main text):

$$P(y) = 5 \times 10^{-2} y + 2000; \text{ where } y \le 20{,}000 \text{ m (equation 6a)}$$

$$P(y) = -1.25 \times 10^{-1} y + 500; \text{ where } 20{,}000 \text{ m} < y < 40{,}000 \text{ m (equation 6b)}$$

$$P(y) = 500; \text{ where } y \ge 40{,}000 \text{ m (equation 6c).}$$

The rainfall rate is given in mm/yr in Equations 6a-c, and *y* is given in meters. In the region closest to the mountain front (Equation 6a), the rainfall rate increases from 2,000 mm/yr to 3,000 mm/yr. In the middle region (Equation 6b), the rainfall rate decreases from 3,000 mm/yr to 500 mm/yr. In the back region (Equation 6c), the rainfall rate remains constant at 500 mm/yr.

We consider two different spatial rock uplift patterns in our non-steady-state experiments. The first is uniform rock uplift at a rate of 1.0 mm/yr. The second, referred to as the ramp uplift pattern, divides the landscape into two rock uplift regions:

$$U(y) = 3.0 \times 10^{-5} y + 0.1; \text{ where } y \le 30{,}000 \text{ m (equation 7a)}$$

$$U(y) = 1.0; \text{ where } y > 30{,}000 \text{ m (equation 7b).}$$

The uplift rate is given in mm/yr in Equations 7a and b, and y is given in meters. We consider changes in uplift rate only in the direction perpendicular to the mountain front, hence the uplift rate varies only in the y direction. In the front of the range, the uplift rate increases linearly from 0.1 to 1.0 mm/yr (Equation 7a). In the back of the range, the uplift rate has a uniform value of 1.0 mm/yr (Equation 7b).

DESCRIPTION OF SUPPLEMENTAL FIGURES

The supplemental figures illustrate channel profiles, k_{sn} patterns, and slope area data for each of the non-steady numerical experiments (X3–X8). Channel slope patterns, which determine the shape of a channel profile, are highly sensitive to the distribution of drainage area along a channel. Two profiles from different river networks can appear different even if they have the same slope-area relationship, simply because the accumulation of drainage area differs between the two channels. For easier comparison between the modeled and Bolivian channels, we create a synthetic transverse and frontal profile. The synthetic channels have the same upstream distance and area-distance relationship as the illustrated Bolivian transverse and frontal channels, but their slopes are set by the modeled k_{sn} values at the same perpendicular distance from the escarpment front (or open boundary in the model).

REFERENCES CITED

Aalto, R., Dunne, T., and Guyot, J.L., 2006, Geomorphic controls on Andean denudation rates: The Journal of Geology, v. 114, no. 1, p. 85–99, doi:10.1086/498101.

Baldwin, J.A., Whipple, K.X., and Tucker, G.E., 2003, Implications of the shear stress river incision model for the timescale of postorogenic decay of topography: Journal of Geophysical Research. Solid Earth, v. 108, no. B3, p. 2158, doi:10.1029/2001JB000550.

Chatanantavet, P., and Parker, G., 2006, Modeling the bedrock river evolution of western Kaua'i, Hawai'i, by a physically-based incision model based on abrasion, *in* Parker, G., and Garcia, M., eds., River, Coastal and Esuarine Morphodynamics; RCEM 2005, Volume 1, Taylor & Francis Group, p. 99–110.

Crosby, B. T., Whipple, K. X., Gasparini, N. M., and Wobus, C. W., 2007, Formation of fluvial hanging valleys: Theory and simulation: Journal of Geophysical Research-Earth Surface, v. 112, no. F3.

Gasparini, N. M., Whipple, K. X., and Bras, R. L., 2007, Predictions of steady state and transient landscape morphology using sediment-flux-dependent river incision models: Journal of Geophysical Research-Earth Surface, v. 112, no. F3.

Howard, A.D., 1994, A detachment-limited model of drainage-basin evolution: Water Resources Research, v. 30, no. 7, p. 2261–2285, doi:10.1029/94WR00757.

Safran, E.B., 1998, Channel network incision and patterns of mountain geomorphology [Ph.D. thesis]: University of California, Santa Barbara.

Tucker, G.E., and Whipple, K.X., 2002, Topographic outcomes predicted by stream erosion models: Sensitivity analysis and intermodal comparison: Journal of Geophysical Research. Solid Earth, v. 107, no. B9, doi:10.1029/2001JB000162.

Tucker, G., Lancaster, S., Gasparini, N., and Bras, R., 2001a, The Channel-Hillslope Integrated Landscape Development Model (CHILD), *in* Harmon, R., and Doe III, W., eds., Landscape Erosion and Evolution Modeling: New York, Kluwer Academic/Plenum Publishers.

Tucker, G.E., Lancaster, S.T., Gasparini, N.M., Bras, R.L., and Rybarczyk, S.M., 2001b, An object-oriented framework for distributed hydrologic and geomorphic modeling using triangulated irregular networks: Computers & Geosciences, v. 27, no. 8, p. 959–973, doi:10.1016/S0098-3004(00)00134-5.

Whipple, K.X., and Tucker, G.E., 1999, Dynamics of the stream-power river incision model: Implications for height limits of mountain ranges, landscape response timescales, and research needs: Journal of Geophysical Research. Solid Earth, v. 104, no. B8, p. 17661–17674, doi:10.1029/1999JB900120.

Whipple, K.X., and Tucker, G.E., 2002, Implications of sediment-flux-dependent river incision models for landscape evolution: Journal of Geophysical Research. Solid Earth, v. 107, no. B2, p. 2039, doi:10.1029/2000JB000044.

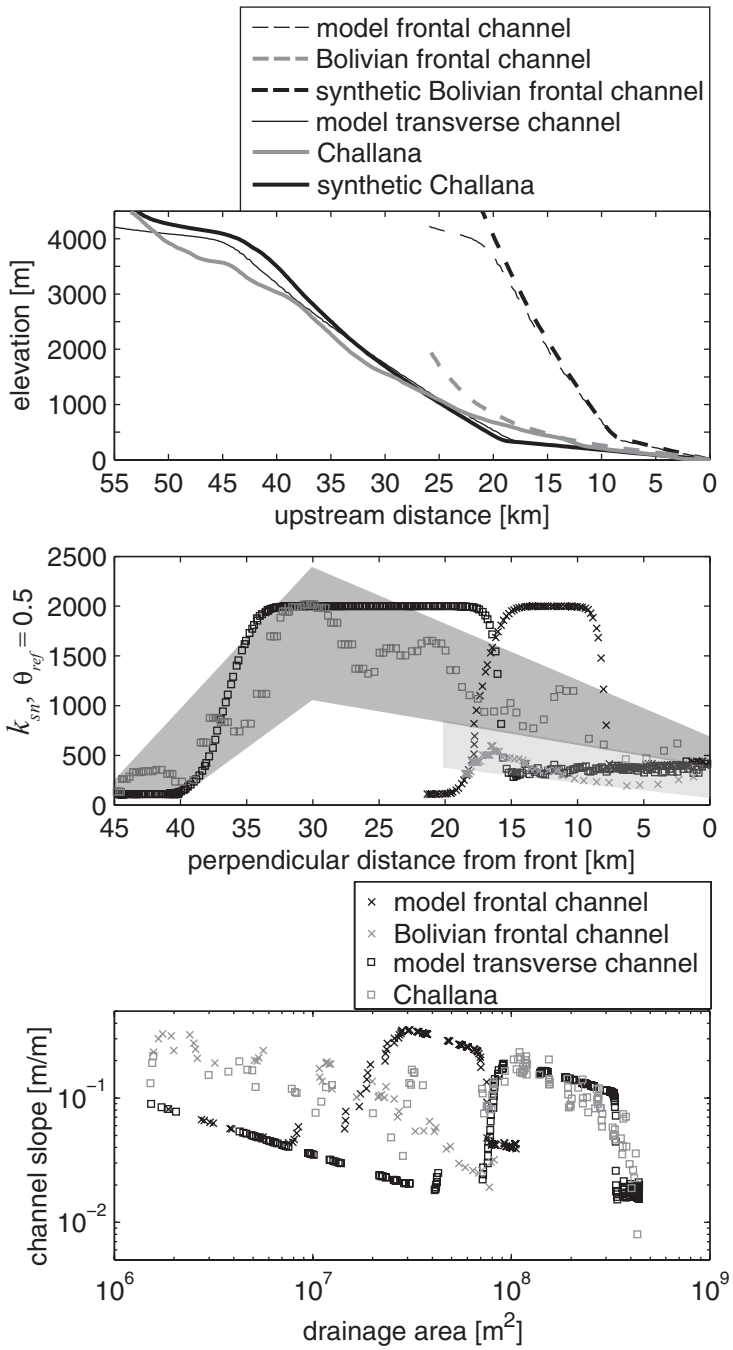

Supplemental Figure 1. From top to bottom, channel profiles, channel steepness index versus perpendicular distance from front, and slope-area data from experiment X3 with low K, K_t values in which rainfall is uniform and uplift decreases through time after a period with uniform uplift (black lines and symbols) and Bolivian data (gray lines and symbols). The locations of the model channels are shown in Figure 11 of the main text. The same legend applies for the bottom two plots and is shown between these plots. Only data across the Beni Escarpment are shown for the Bolivian channels. The dark-gray and light-gray bands in the channel steepness plot represent the range of channels steepness values observed in the high k_{sn} Bolivian transverse channels and the frontal channels, respectively. These same bands are shown in Figure 7 of the main text, but because the reference concavity value is different in this figure, the channel steepness values are not the same as those shown in Figure 7 of the main text.

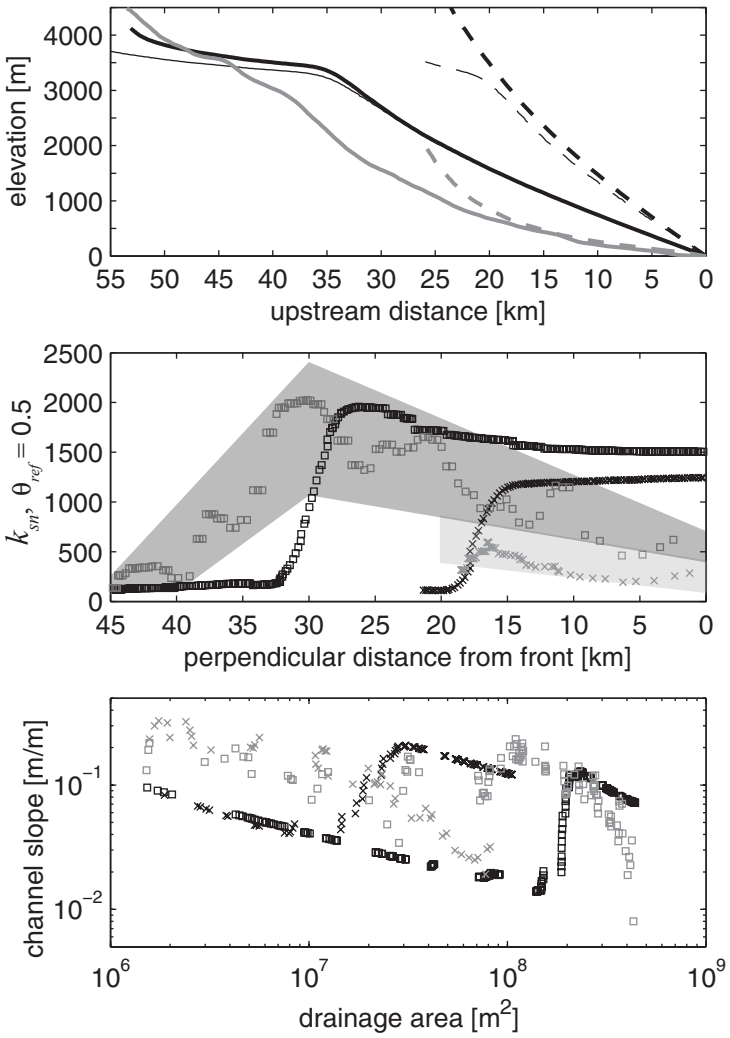

Supplemental Figure 2. From top to bottom, channel profiles, channel steepness index versus perpendicular distance from open boundary or mountain front, and slope-area data from experiment X4 with low K, K_t values, non-uniform rainfall and a uniform uplift increase (black lines and symbols) and Bolivian data (gray lines and symbols). For legends and details see the caption for Supplemental Figure 1.

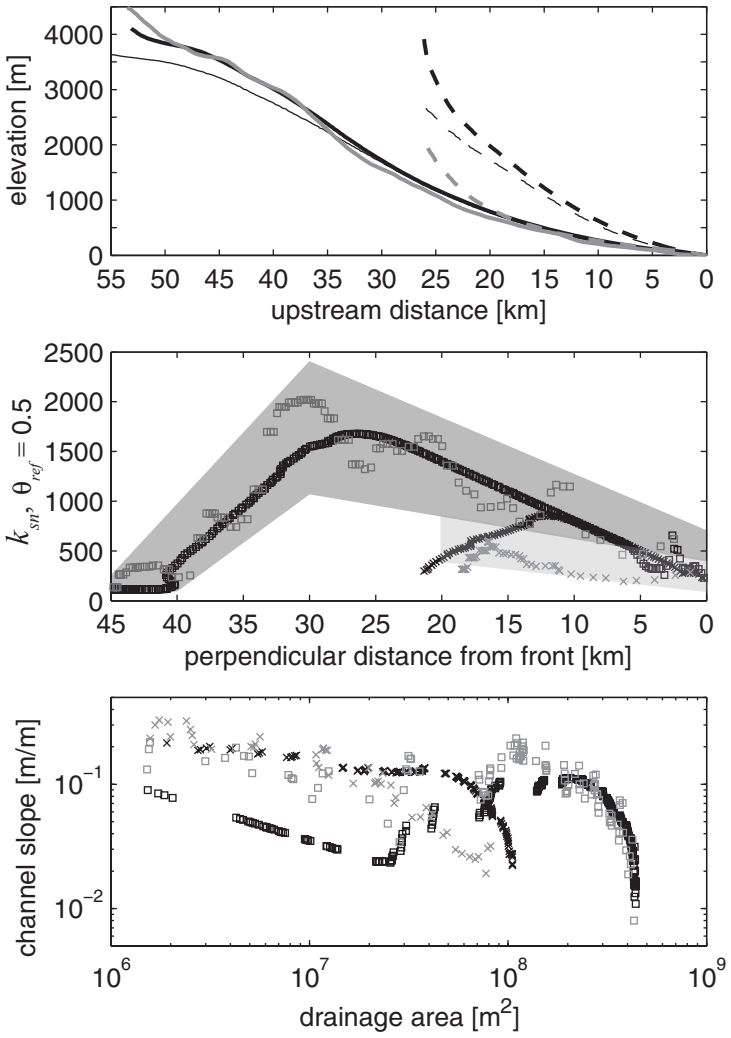

Supplemental Figure 3. From top to bottom, channel profiles, channel steepness index versus perpendicular distance from open boundary or mountain front, and slope-area data from experiment X5 with low K, K_t values, uniform rainfall and ramp uplift pattern (black lines and symbols) and Bolivian data (gray lines and symbols). For legends and details see the caption for Supplemental Figure 1.

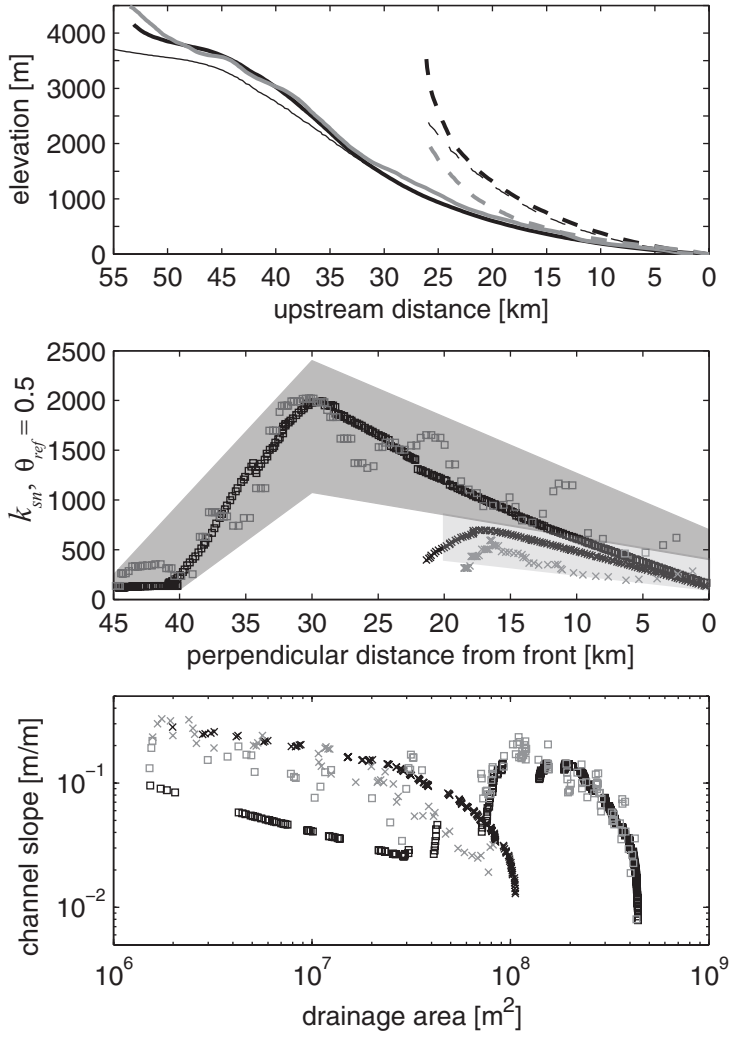

Supplemental Figure 4. From top to bottom, channel profiles, channel steepness index versus perpendicular distance from open boundary or mountain front, and slope-area data from experiment X6 with low K, K_t values, non-uniform rainfall and ramp uplift pattern (black lines and symbols) and Bolivian data (gray lines and symbols). For legends and details see the caption for Supplemental Figure 1.

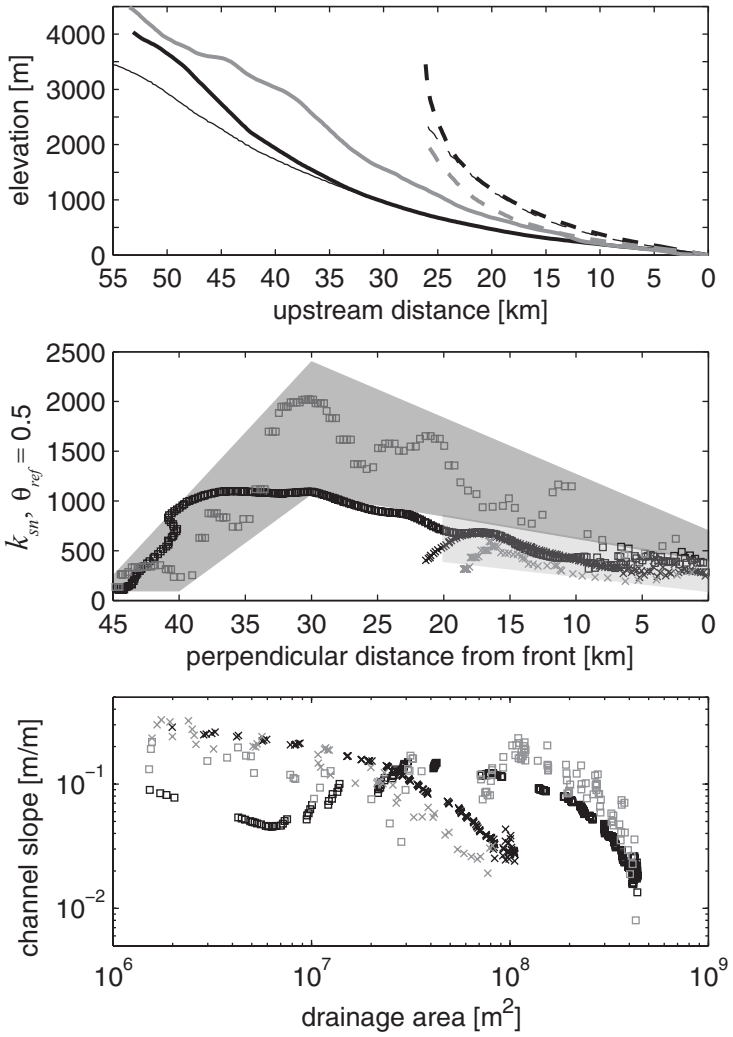

Supplemental Figure 5. From top to bottom, channel profiles, channel steepness index versus perpendicular distance from open boundary or mountain front, and slope-area data from experiment X7 with high K, K_t values, uniform rainfall and ramp uplift pattern (black lines and symbols) and Bolivian data (gray lines and symbols). For legends and details see the caption for Supplemental Figure 1.

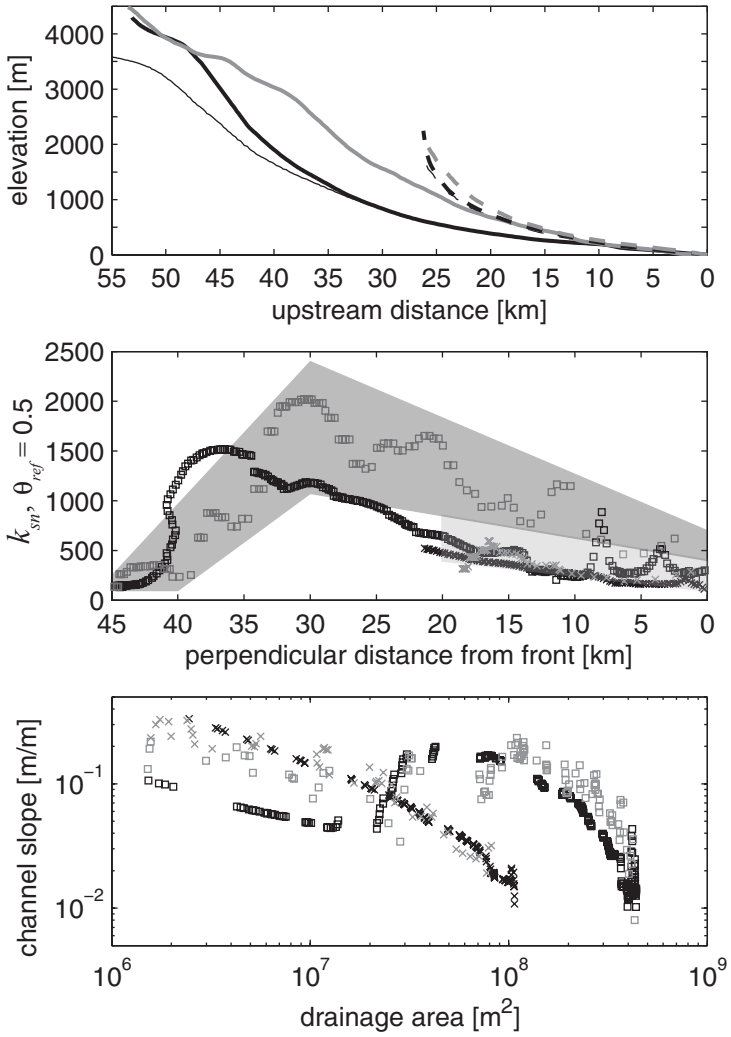

Supplemental Figure 6. From top to bottom, channel profiles, channel steepness index versus perpendicular distance from open boundary or mountain front, and slope-area data from experiment X8 with high K, K_t values, non-uniform rainfall and ramp uplift pattern (black lines and symbols) and Bolivian data (gray lines and symbols). For legends and details see the caption for Supplemental Figure 1.